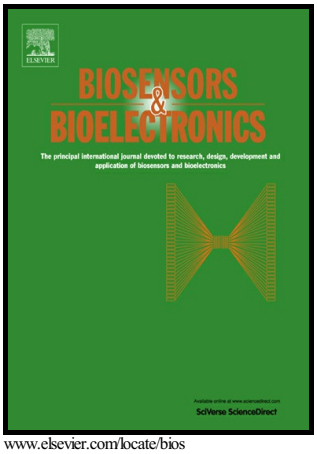

www.elsevier.com/locate/bios

Magnetic field-assisted SPR biosensor based on carboxyl-functionalized graphene oxide sensing film and Fe_3O_4-hollow gold nanohybrids probe

Qiong Wu, Ying Sun, Di Zhang, Shuo Li, Xinghua Wang, Daqian Song

PII: S0956-5663(16)30564-4
DOI: http://dx.doi.org/10.1016/j.bios.2016.06.035
Reference: BIOS8827

To appear in: *Biosensors and Bioelectronic*

Received date: 7 April 2016
Revised date: 12 June 2016
Accepted date: 13 June 2016

Cite this article as: Qiong Wu, Ying Sun, Di Zhang, Shuo Li, Xinghua Wang and Daqian Song, Magnetic field-assisted SPR biosensor based on carboxyl functionalized graphene oxide sensing film and Fe_3O_4-hollow gold nanohybrid probe, *Biosensors and Bioelectronic* http://dx.doi.org/10.1016/j.bios.2016.06.035

Magnetic field-assisted SPR biosensor based on carboxyl-functionalized graphene oxide sensing film and Fe_3O_4-hollow gold nanohybrids probe

Qiong Wu, Ying Sun, Di Zhang, Shuo Li, Xinghua Wang, Daqian Song*

College of Chemistry, Jilin University, Qianjin Street 2699, Changchun 130012, P.R. China

*Corresponding author: Daqian Song. Tel.: +86 431 85168399; fax: +86 431 85168399. E-mail address: songdq@jlu.edu.cn

Abstract

A novel surface plasmon resonance (SPR) biosensor, coupled with the magnetic bioseparation technique, was constructed and used to the determination of human IgG. Carboxyl-functionalized graphene oxide (cGO) sheet was employed as the sensing film for the efficient immobilization of capture antibody (Ab_1). Nanoconjugates ($FHAb_2$), obtained by binding detection antibody (Ab_2) to the nanohybrids containing Fe_3O_4 nanoparticles (Fe_3O_4 NPs) and hollow gold sphere nanoparticles (HGNPs), were used to specifically collect the target analytes from sample solutions and serve as labels. Owing to the notable plasmonic fields spreading over inner and outer surfaces, HGNPs played key roles in amplifying the SPR response signals originating from the dielectric changes on the sensing films during the binding of Ab_1 and

human IgG-Ab_2FH complexes. In addition, $FHAb_2$ were also used as "vehicles" for the rapid delivery of the separated and enriched target analytes from sample solutions to the sensor surface via an external magnet. In the present method, taking advantages of the magnetic field-driven mass transfer and the significant signal amplification effect of $FHAb_2$, the separation and analysis of human IgG in serum samples are quite effective and sensitive. The limit of detection was 1.88 ng mL^{-1}, which is about 260-fold lower than that obtained by routine SPR biosensors with sandwich assay.

Keywords: Surface plasmon resonance (SPR) biosensor; Hollow gold sphere nanoparticles; Fe_3O_4 nanoparticles; Carboxyl-functionalized graphene oxide; Magnetic field

1. Introduction

Surface plasmon resonance (SPR) biosensor is an advanced analysis tool based on the changes in the refractive index of material on the metal surface. SPR biosensors enable the label-free and real-time detection, providing rich information on the specificity, affinity, and kinetics of biomolecular interactions (Li et al., 2012), which makes them be attractive tools in food analysis (Atar et al., 2015), biochemistry (Wang et al., 2016), clinical diagnosis (Eletxigerra et al., 2016) and environmental monitoring (Kamaruddin et al., 2016).

In 1998，colloidal gold was incorporated into SPR immunosensing for the first time, which brought significant advances in both generality and sensitivity of SPR sensors (Lyon et al., 1998). The development of this technology was rapid in recent years, and various gold nanostructures such as gold sphere nanoparticles (Springer et al., 2014), gold nanorod (Zhang et al., 2015), gold nanobipyramid (Zhang et al., 2014), gold nanostar (Mariani et al., 2015) and hollow gold nanoparticles (Zhong et al., 2014) have been introduced to primarily expand the application range and improve the sensitivity of SPR sensors. With the advantages of low density, high specific surface area, and reduction of costs (Liu et al., 2010), hollow gold nanoparticles (HGNPs) could be utilized to improve the performances of SPR biosensors instead of their solid counterparts with similar dimensions (Mahmoud et al., 2014), which offers HGNPs more potential in SPR technology.

Iron oxide nanoparticles (Fe_3O_4 NPs) as magnetic nanomaterial, have been demonstrated to be promising in biomaterials immobilization (Baghayeri et al., 2014), bioseparation (Mahmoud et al., 2015), environmental treatment (Wang et al., 2015), biomedical and bioengineering usage (Singh et al., 2015), and food analysis (Wu et al., 2016). Especially, the application of biofunctionalized Fe_3O_4 NPs in biosensing has attracted great focus owing to the good properties of biofunctionalized Fe_3O_4 NPs including high specific surface for

biomolecule immobilization and good water solubility. Most researchers utilized magnetic particles for: (1) separation, purification and concentration of analytes in complex samples with the help of external magnets, avoiding the procedure of centrifugation and minimizing the matrix effects (Yao et al., 2013); (2) capture of modified magnetic particles on the sensing surface directly by a magnetic pillar, simplifying the procedures of analysis and regeneration of biosensors (Sun et al., 2007). Sensitivity of biosensors could be effectively enhanced by using magnetically driven carriers since mass transfer of analytes to the sensor surface is usually hindered by the low diffusion speeds of analytes in regular pattern. However, only a few papers reported the application of Fe_3O_4 NPs as carriers to the rapid delivery of analytes from a sample solution to the sensor surface by external magnetic field (Wang et al., 2011).

SPR is highly sensitive to the changes in effective refractive index, thickness and mass of the test medium in the vicinity of the metal surface (Wang et al., 2010). Therefore, Fe_3O_4 NPs with high refractive index and large mass effects have attracted considerable interest on fabricating SPR biosensors (Liu et al., 2014; Chen et al., 2014; Garibo et al., 2014). Moreover, multifunctional Fe_3O_4-gold nanoparticles hybrid materials have also been employed in preparing multimode platforms for biomedical applications by utilizing the comprehensive properties of

Fe_3O_4 and gold nanoparticles (Hoskins et al., 2012).

Inspired by the reported works listed above, here we constructed a SPR biosensor using biofunctionalized Fe_3O_4-HGNPs nanohybrids (FH) as labels and carboxyl-functionalized graphene oxide (cGO) as sensing film. SPR biosensor technology and magnetic bioseparation were combined for the detection of human IgG. cGO sheets were assembled on gold film using MEA as bridging agent, and capture antibody (Ab_1) was immobilized on folded cGO sheets. Nanoconjugates ($FHAb_2$), obtained by binding detection antibody (Ab_2) to the FH, were employed as selective collectors to separate and concentrate human IgG in sample solutions. The concentrated human IgG-Ab_2FH were rapidly delivered to the sensing surface and interacted specifically with Ab_1 immobilized on the sensor with the help of an external magnetic field. A schematic diagram of the experimental procedure is shown in Fig. 1.

2. Materials and Methods

2.1 Materials

Human IgG, rabbit anti-human IgG, mouse IgG, and bovine IgG were purchased from Beijing Boisynthesis Biotechnology Company. Bovine serum albumin (BSA) was purchased from Ding Guo Biotechnology Company. Chicken serum was purchased from Shanghai Jonln Industrial Company. Hydrogen tetrachloroauratehydrate

($HAuCl_4 \cdot 3H_2O$) was purchased from Acros. 3-Mercaptopropinic acid (MPA), 1-ethyl-3-(3-dimethylaminopropyl) carbodiimide (EDC) and N-hydroxysuccinimide (NHS) were purchased from Jkchemical. L-Cysteine (L-Cys), (3-aminopropyl)triethoxysilane (APTES), cobalt chloride hexahydrate ($CoCl_2 \cdot 6H_2O$), sodium borohydride ($NaBH_4$), sodium citrate and ethanol were purchased from Sinopharm Chemical Reagent Co., Ltd. All chemicals were of analytical grade and used without further purification. All water used in the syntheses was prepared using a Millipore purification device.

Rabbit anti-human IgG, human IgG, mouse IgG and bovine IgG were stored at -20 °C and other reagents were stored at 4 °C. Sodium phosphate buffered saline (PBS, 0.01 mol L^{-1}, pH 7.4) was used as the running buffer.

2.2 Equipment

A wavelength-modulation SPR biosensor installed by our research group was used in this work (Fig. S1). It consists of an iodine-tungsten lamp, a light guide system, a prism-sensing unit, a flow cell reactor, a miniature spectrometer and a data-processing system. The light emitting from the iodine-tungsten lamp was parallized and polarized by a collimator combined with a polarizer, then was guided to an optical prism

equipped with a SPR chip to excite surface plasmon at the interface of the metal and the sample solution. The resonant wavelength was determined by using a miniature fiber optical spectrometer (HR2000+, Ocean Optics Inc., USA). The binding between the receptors immobilized on sensing film and the analytes dissolved in solution can induce the change in the refractive index of gold film surface, which will result in the variation of the resonant peak position in SPR spectrum. The values of observed resonant wavelength shifts were recorded and analyzed to obtain the information of the binding between receptors and analytes.

2.3 Preparation of Fe_3O_4-HGNPs-Ab_2 bioconjugates

Fe_3O_4 NPs were prepared by a chemical coprecipitation method (Zhang et al., 2014). The obtained Fe_3O_4 NPs were functionalized with amine groups through the silanization reaction using APTES (Eslamipour and Hejazi, 2015). HGNPs were synthesized according to Schwartzberg's report (Schwartzberg et al., 2006).

50 µL of 1 mg mL^{-1} L-Cys solution was added into 1 mL of HGNPs solution. The mixture was kept for 3 h. Subsequently, 0.5 mL of EDC and NHS mixture (7.5 mM: 1.5 mM) was added as coupling reagents, and the mixture was incubated for 30 min to activate the –COOH groups of L-Cys. 150 µL of amine-modified Fe_3O_4 NPs solution was diluted with

DI-water to a volume of 1 mL, and was added dropwise to the mixture under sonicating in 30 min. The obtained mixture underwent vortex vibration for another 3 h. The produced amine-functionalized nanohybrids were isolated and washed with ethanol and DI-water using a permanent magnet as collector. Then, the nanohybrids were immersed in 5 mL of 2% glutaraldehyde ethanol solution, and were stirred for 3 h at room temperature to obtain the aldehyde-modified nanohybrids. The obtained nanohybrids were isolated by magnetic separation and washed with PBS for 3 times to remove unreacted glutaraldehyde. Finally, the aldehyde-activated magnetic nanohybrids (FH) were redispersed in 3 mL of PBS. 400 μg of Ab_2 was added into the aldehyde-activated FH solution under soft stirring. The mixture was kept at 4 °C for 12 h to permit the binding of Ab_2 with aldehyde-activated FH through interaction between $–NH_2$ residues of Ab_2 and the –CHO groups of aldehyde-activated FH. Finally, the obtained $FHAb_2$ were separated by magnetic separation, followed by washing with PBS and PBS containing 1.0 wt% BSA in sequence to remove the unbound Ab_2 and block the nonbinding sites, respectively. The isolated $FHAb_2$ were dissolved in 3 mL of PBS and stored at 4 °C for further use. The Fe_3O_4-Ab_2 bioconjugate was also prepared by the similar procedure for comparison.

2.4 Modification of the sensing chip

cGO was employed as a supporter for the immobilization of Ab_1 because of its great capability for immobilizing proteins, which has been demonstrated in our previous work (Wu et al., 2016). 10 mM MEA was injected into the reactor, followed by incubating for 1 h to modify the surface of the gold film with amino groups. Subsequently, 1 mg mL^{-1} cGO was injected into the reactor and assembled on the gold film via electrostatic interaction. Then the mixture of NHS/EDC (1.5 mM: 7.5 mM) was injected to activate the carboxyl groups of cGO. 20 min later, PBS was injected to wash off the excess NHS/EDC and balance the baseline of SPR signals. Then, Ab_1 was injected into the reactor, followed by 12 h incubation to allow the sufficient immobilization of Ab_1 on cGO sheets. PBS was injected again to wash off unbound Ab_1, and 1 M ethanolamine hydrochloride (pH 8.0) was injected as sealant to block the non-specific binding sites on cGO sheets.

2.5 Detection of human IgG in different approaches

The detection of human IgG was performed in four approaches (Fig. 1, A–D). In approach A, human IgG with different concentration was separately injected into the reactor. After 40 min, 40 μg mL^{-1} Ab_2 was injected into the reactor, followed by incubation for 30 min. Then PBS was flowed over the sensing platform to remove the unbound Ab_2, and

the final resonant wavelength shift was recorded. The detection procedure of approach B consists of two steps： Firstly, Fe_3O_4-Ab_2 bioconjugate was added into human IgG solution, and the final volume of the mixture was adjusted to 4 mL by PBS. The mixture was slightly shaken for a few seconds and kept for 3 h at 4 °C. Secondly, the obtained Fe_3O_4-Ab_2-IgG conjugates were isolated by magnetic separation and redispersed in 400 μL of PBS. That is to say, the enrichment ratio ($volume_{sample}$/$volume_{PBS}$) is 10 times. The redispersed Fe_3O_4-Ab_2-IgG conjugates were injected into the reactor to interact with Ab_1 immobilized on cGO sheets. After 40 min, PBS was softly flowed over the sensor surface to wash off unbounded Fe_3O_4-Ab_2-IgG conjugates. Under the same conditions, human IgG-Ab_2FH were tested to investigate the effect of HGNPs on sensitivity enhancement (approach C). In approach D, an external magnetic field with a gradient perpendicular to the surface of ∇B = 0.10 T mm^{-1} was placed at a distance of 2 mm from the sensor surface. Time for incubation of human IgG-Ab_2FH solution in the reactor was shortened to 10 min. Afterward, the magnetic field was switched off and PBS was employed again to remove the unbound human IgG-Ab_2FH from the surface of sensing chip. The sensor responses for four approaches were determined as the shifts of resonant wavelength, before the sample injection and after the rinsing with PBS.

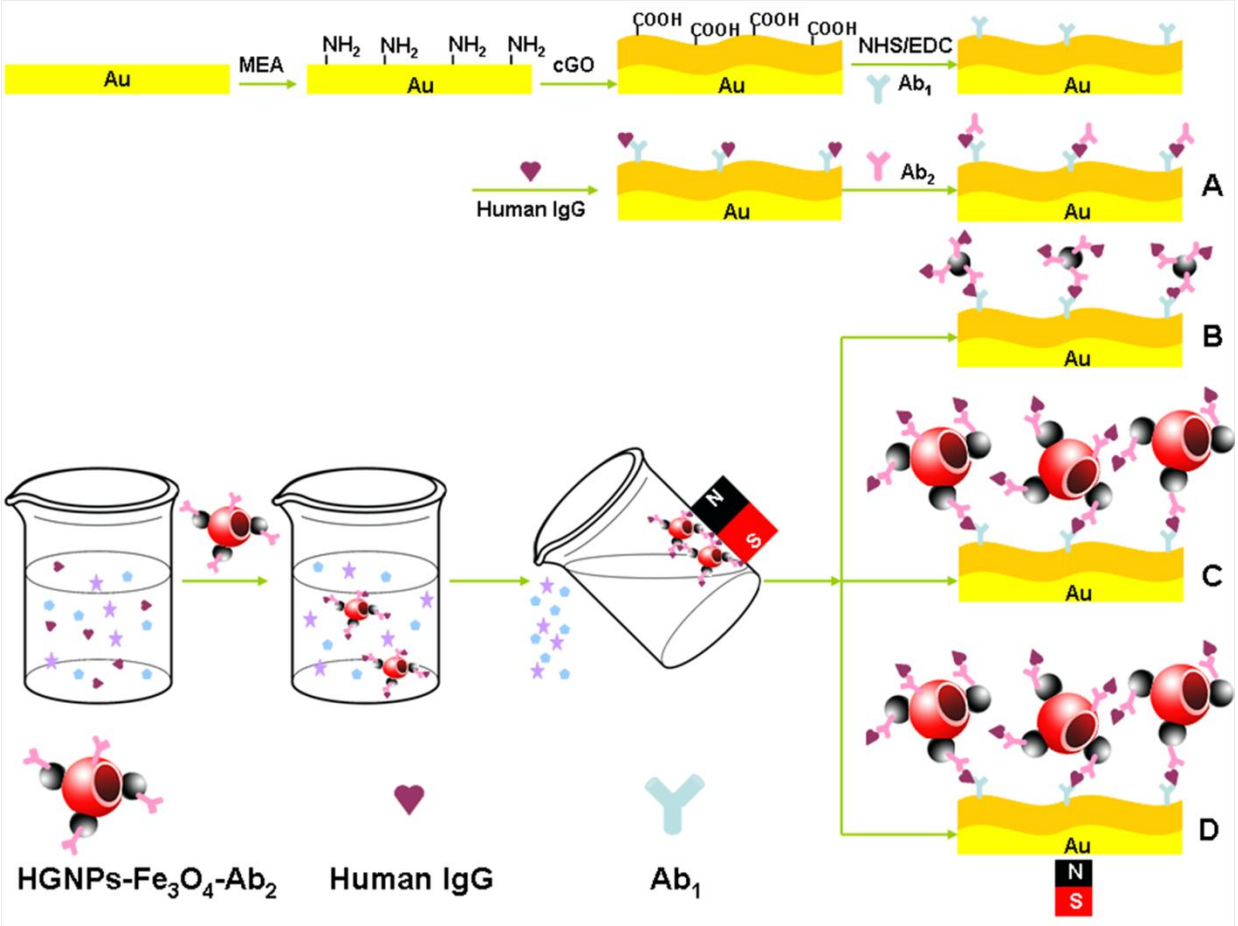

Fig. 1

2.6 Regeneration

After a series of antigen–antibody binding assays were performed, the prism was taken away from the reactor. Then the glass slide with gold film was taken off from the prism. The gold film was gently wiped with cotton dipped in ethanol. Ethanol and DI-water was sequentially used to ultrasonically clean the swabbed gold films for 20 min to wipe out the cGO-based sensing substrate. Finally, the gold film was dried with gaseous nitrogen. When the slide with gold film was reused, the resonant wavelength returned to the baseline.

3. Results and discussions

3.1 Characterization of $FHAb_2$ bioconjugates

The morphology and size distribution of the prepared Fe_3O_4 NPs (Fig. 2a), HGNPs (Fig. 2b) and FH (Fig. 2c) were characterized by transmission electron microscopy (TEM). The TEM image shows that the spherical Fe_3O_4 NPs have a size range of 8−11 nm in diameter with slight aggregation due to the high surface energy (Fig. 2a). The TEM image shown in Fig. 2b reveals that the HGNPs were of well structure and good monodispersity with average shell diameter of 44 ± 5 nm and wall thickness of 3 ± 0.6 nm. From Fig. 2c, it could be clearly observed that the FH were successfully prepared and HGNPs distribute well in Fe_3O_4 NPs piles.

The applicability of magnetic separation of the obtained FH was demonstrated by fitting FH suspension in the absence and presence of an external magnet (Fig. 2d). Suspension of the superparamagnetic FH was homogeneous in the absence of an external magnetic field. However, the homogeneity of the suspension was broke upon applying an external magnetic field. It was observed that FH in the suspension moved fast toward the magnet and the bulk solution became clear and transparent. The applicability of magnetic separation ensures FH and its bioconjugates

could be separated easily from matrix in one step by using an external magnetic field.

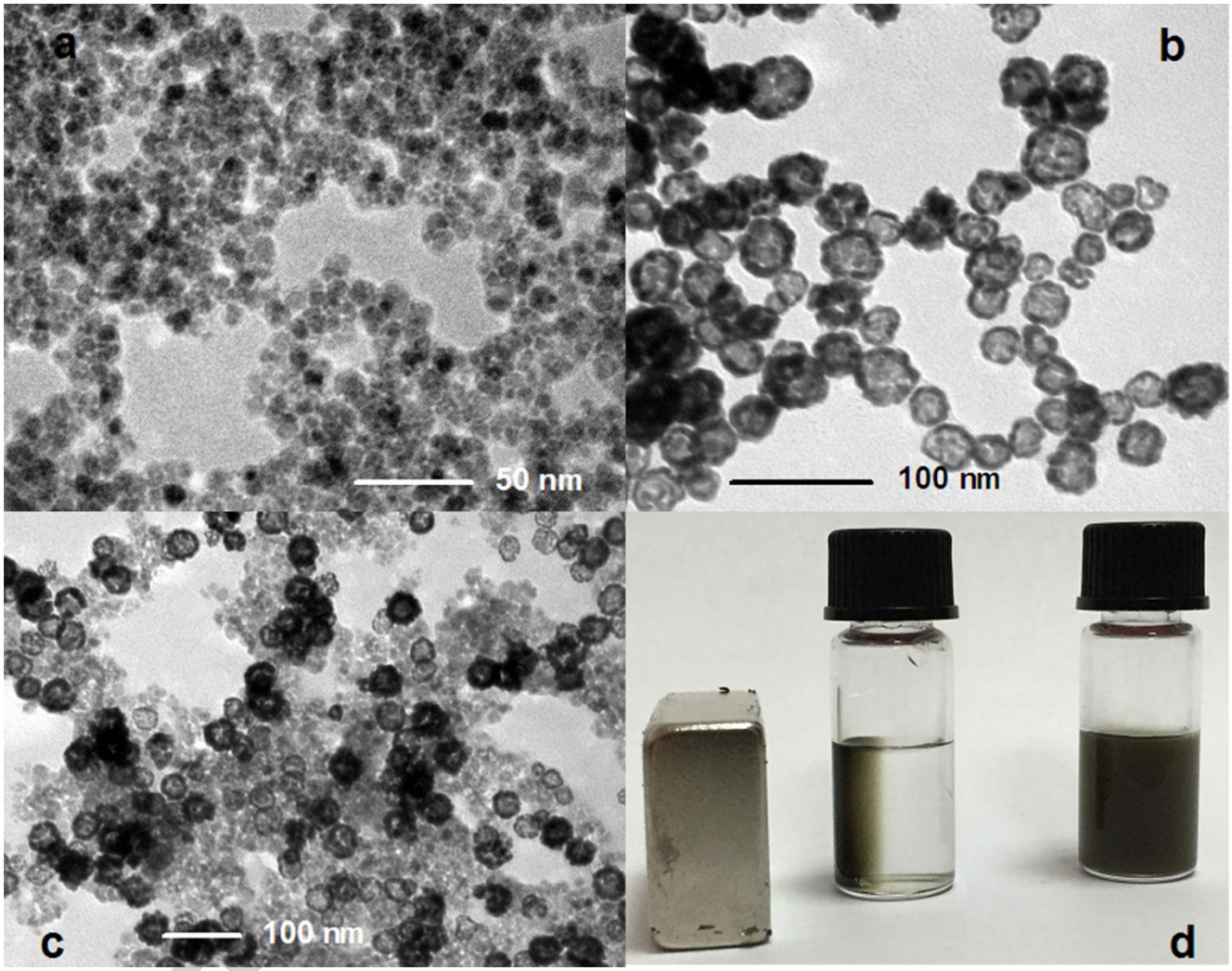

Fig. 2

Furthermore, the magnetic properties of Fe_3O_4 NPs and FH were investigated particularly via a SQUID magnetometer. The mass

magnetization curves of superparamagnetic Fe_3O_4 NPs and FH versus the applied magnetic field by cycling the field between -60 and 60 kOe are displayed in Fig. 3. The saturated mass magnetizations of Fe_3O_4 NPs and FH at 300 K were 72 emu g^{-1} and 58 emu g^{-1}, respectively. The decrease of saturated mass magnetization from Fe_3O_4 NPs to FH should be attributed to the adding mass of HGNPs.

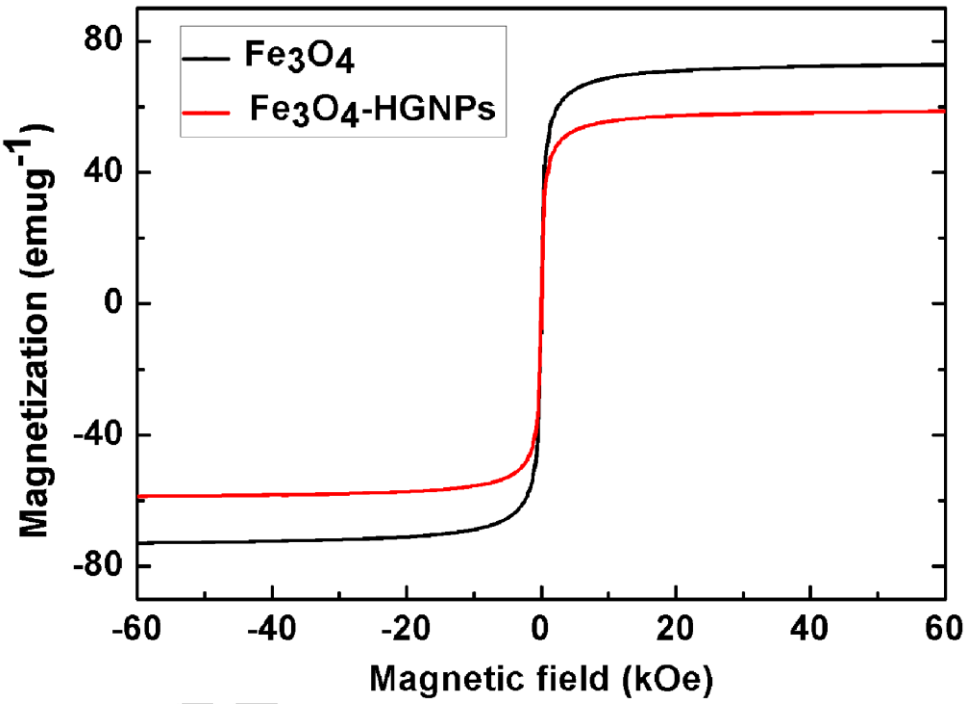

Fig. 3

In addition, the components of FH were confirmed through X-ray photoelectron spectroscopy (XPS) analysis. The binding energy of C (1 s) at 284.8 eV was used as an internal reference. It can be seen from Fig.

S2a that the Au 4f spectrum is resolved into two spin-orbit components. The two peaks occurring at the binding energies of 83.9 eV and 87.5 eV, are consistent with Au $4f_{7/2}$ and $4f_{5/2}$ peak of metallic gold, respectively (Hedman et al., 1971; Turner and Single, 1990). The two peaks of Fe 2p spectrum shown in Fig. S2b occur at the binding energies of 710.4 eV and 723.9 eV, corresponding to Fe $2p_{3/2}$ and Fe $2p_{1/2}$, respectively (Marcus and Grimal, 1992; Tan et al., 1990). The contents of gold and Fe elements existing in FH are listed in Table. S1 and the calculating results indicate the mass ratio of Fe_3O_4 NPs and HGNPs is 4.1: 1.

UV-Vis absorption spectra of Fe_3O_4 NPs, HGNPs, FH and $FHAb_2$ conjugates are shown in Fig. 4. The absorbance of Fe_3O_4 NPs decreased monotonically with the increase of incident light wavelength in the range of 450−1000 nm and no obvious absorption peak was observed (curve a). After the conjugating of Fe_3O_4 NPs and HGNPs, due to the introduction of HGNPs (curve b), a new absorption peak located at 597 nm appeared (curve c) indicating the formation of FH. A significant red-shift (612 nm, curve d) of absorption peak occurred after excess Ab_2 was added into the activated FH solution. This red-shift illustrates the localized refractive index near the FH surfaces changed, which indirectly indicates the immobilization of Ab_2 on the FH surfaces.

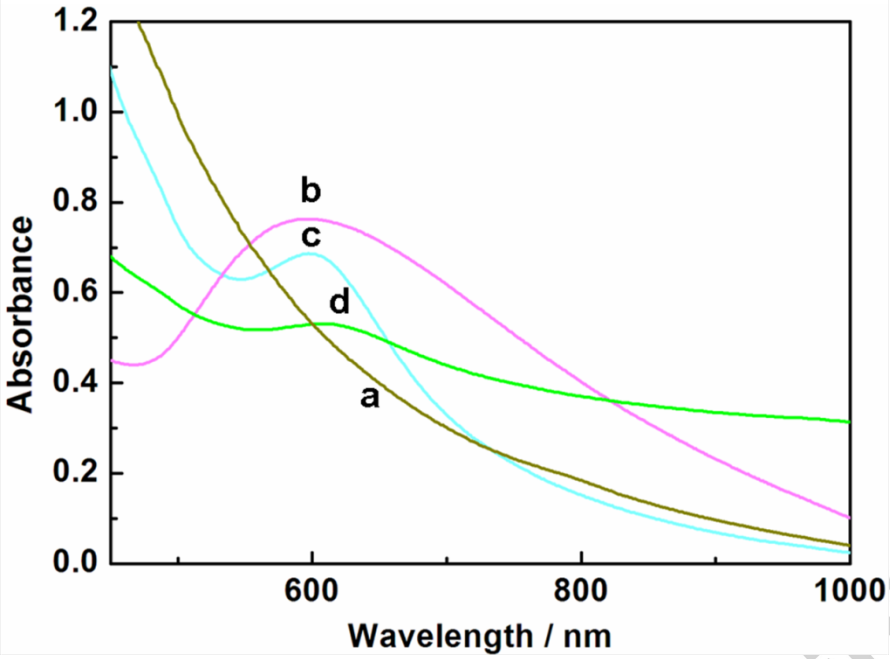

Fig. 4

3.2 Fabrication of biosensing film

cGO was selected to immobilize Ab_1 considering that the abundant carboxyl groups existing its surface are beneficial to immobilize antibody. The optimal concentration of Ab_1 was selected by measuring shifts of resonant wavelength when gradient concentration of Ab_1 was separately flowed over the sensing chip. The resonant wavelength moves to the longer wavelength with the increase of the concentration of Ab1 (Fig. 5a). The maximum resonant wavelength shifts for the Ab_1 immobilization at concentrations of 125 and 150 μg mL^{-1} are almost the same, which indicates that antibody immobilized on cGO sheets reaches saturation. As relatively high concentration of antibodies might result in stereo hindrance, 125 μg mL^{-1} is selected as the optimal Ab_1 concentration with

the maximum resonant wavelength shifts of 13.2 nm. To evaluate the immobilizing ability of cGO for Ab_1, the sensing film based on cGO and MPA was separately tested in approach A and the obtained results were shown in Fig. S3. The SPR biosensor based on MPA and cGO respectively show good responses to human IgG in the concentration ranges of 1-32 μg mL^{-1} and 0.5-32 μg mL^{-1}, with the corresponding resonant wavelength shifts of 0.20-2.3 nm and 0.20-3.8 nm.

3.3 $FHAb_2$ enhanced detection for human IgG

The amount of the $FHAb_2$ is crucial since $FHAb_2$ simultaneously served as collectors to separate target analytes from sample solutions and labels to amplify the response signals. Therefore, the effect of the volume of $FHAb_2$ solution was tested on the SPR response with the concentration of human IgG setting to 4 μg mL^{-1} (Fig. S4). Human IgG-Ab_2FH solutions were collected by using different amount of $FHAb_2$. After human IgG-Ab_2FH solutions were injected, the resonant wavelength shifts increase with the increase of the amount of $FHAb_2$ and reaches maximum when the volume of $FHAb_2$ solution was set as 230 μL, and then trends to be stable. This result suggests that human IgG-Ab_2FH transferred to gold film reached saturation when the volume of $FHAb_2$ solution was 230 μL. Insufficient $FHAb_2$ would decrease the amount of

binding human IgG in collecting step, and result in smaller signal amplification effect in measurement. On the contrary, excess $FHAb_2$ would lead to the waste of Ab_2 and poor accessibility of Ab_1 when $FHAb_2$ were transferred to the sensing film due to the stereo hindrance. Therefore, 230 μL is selected as the optimal volume of the $FHAb_2$ solution.

Under the optimized experimental conditions, the concentrated human IgG-Ab_2FH with various human IgG amount are separately analyzed by approach D (Fig. 1). The collected human IgG-Ab_2FH from a sample solution could be transferred to the Ab_1/cGO/gold film on the sensor surfaces within 10 min via a magnet fixed under the reactor. After the magnet was removed, PBS was injected to rinse the sensing film. It should be noted that the minimum resonant wavelength shift is 0.20 nm, which is limited by the spectral resolution of the miniature spectrometer built in the SPR biosensor. Therefore, the lowest detectable concentration of human IgG was also limited. The constructed biosensor shows a sensitive response to human IgG in the concentration range of 1.88-1000 ng mL^{-1}, with the minimum and maximum shifts of resonant wavelength 0.2 nm and 16 nm, respectively.

To demonstrate the analytical performance of the present method using approach D, three detection approaches, including routine sandwich assay (approach A), Fe_3O_4-enhanced sandwich assay (approach B) and FH-enhanced sandwich assay (approach C), are designed and tested in

this work. The response signals of human IgG samples with different concentrations obtained by these four approaches are shown in Fig. 5b, and the analytical performance of each approach are listed in Table S2. The lowest detectable concentration of human IgG obtained by approach A, B and C are 500, 30 and 7.5 ng mL^{-1}, which are 260, 16 and 4-fold higher than that obtained by approach D, respectively.

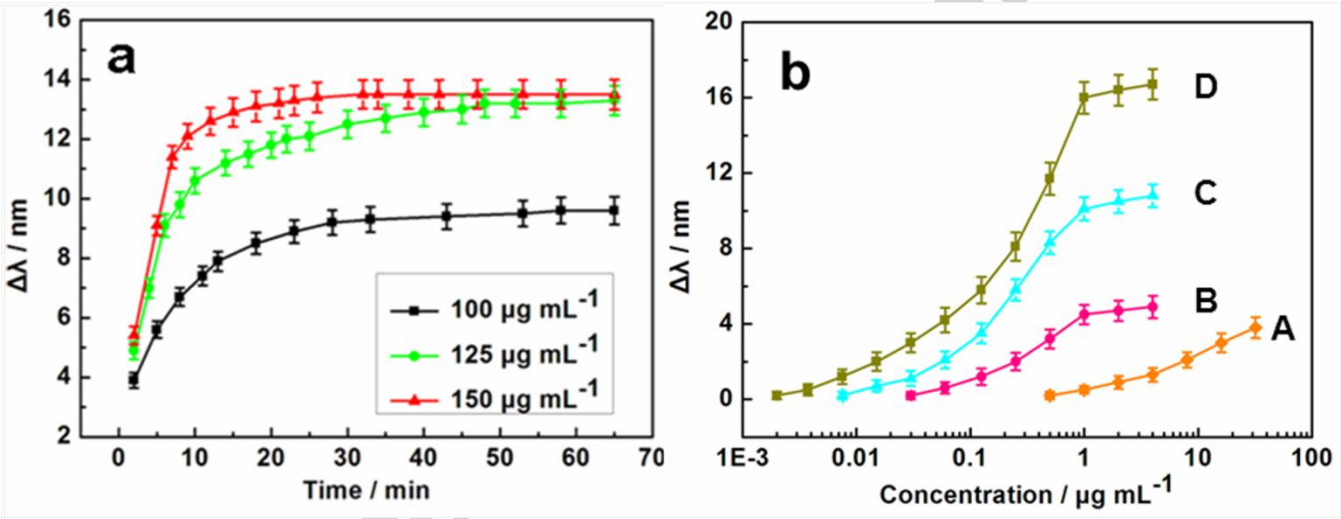

Fig. 5

For the Fe_3O_4-enhanced sandwich assay (approach B), the obtained detection limit is ~ 16-fold lower than that by approach A. The notable enhancement of analytical performance should be credited with the large mass and high refractive index of the Fe_3O_4 NPs and efficient enrichment of human IgG.

In approach C, FH were used to amplify the SPR response and the obtained detection limit is ~ 4-fold lower than that by approach B. The signal amplification of SPR response is achieved by introducing HGNPs. In one respect, a considerable increase in the total mass of FH on the sensing film directly increases the real component value of SPR. In the other respect, the electronic coupling interaction between the localized surface plasmon of HGNPs and the surface plasmon wave associated with the SPR gold films significantly affects the imaginary component of SPR. Moreover, the introduction of HGNPs with large specific surface area offers more binding sites for human IgG.

For the FHAb_2-enhanced sandwich assay (approach C), human IgG-Ab_2FH arrived at the sensing film via low diffusion driven mass transfer, and the sensor response was not saturated during 40 min incubation. Slow diffusion limits the mass transfer of human IgG-Ab_2FH to the sensing film, and results in the insufficient binding of human IgG-Ab_2FH. A significant decrease in detection limit occurred when a magnetic field gradient is applied (approach D), which should be owed to the way of rapid magnetically driven mass transfer.

The SPR spectra for detection of 250 ng mL^{-1} human IgG by approach C and D were shown in Fig. S5. The increase of the resonant wavelength shift obtained by approach C (5.8 nm) and D (8.1 nm) indicates the efficiency improvement of mass transfer benefiting SPR

response.

The great amplification of SPR response and the low detection limit obtained by the fabricated sensor using approach D are attributed to several improvements of sample pretreatment and SPR measurement. The employment of cGO with abundant carboxyl groups as supporter efficiently improves the immobilization of antibodies Ab_1. The enrichment of human IgG by $FHAb_2$ largely decreases the detection limit of this method. And $FHAb_2$ also significantly amplifies the SPR response signals.

For comparison, analytical performance of several reported methods for detecting IgG were listed in Table 1. The detection limits for IgG obtained by different strategies rank from 2 μg mL^{-1} to 1 pg mL^{-1}. The biosensing strategy present in this work offers a relatively lower detection limit. However, limited by the spectral resolution and sensitivity of the miniature spectrometer built in the SPR biosensor used in this work, the obtained detection limit is still higher than that achieved by other groups (Liu et al., 2016; Lynes et al., 2013). From another perspective, the detection limit obtained by the present method is about 260-fold lower than that of routine sandwich assay performed under the same instrumental conditions, which strongly demonstrates the potential of the present method in SPR sensitivity enhancement. In addition, the designed immunosensor suffers less matrix interference, which is beneficial for the

analyses of complex samples.

3.4 Sensor specificity

To evaluate whether there is non-specific affinity between $FHAb_2$ and Ab_1/cGO-based sensing chip, a blank sample without human IgG was analyzed by approach D as a control experiment. The resonant wavelength shift was calculated by recording the resonant wavelengths before a 10-min incubation of $FHAb_2$ under an external magnetic field and after the rinsing sensing surface with PBS. The resulting resonant wavelength shift is close to zero, indicating that the nonspecific interaction between $FHAb_2$ and the sealed surface of sensing chip is negligible.

Mouse IgG and bovine IgG was separately analyzed by the designed SPR biosensor using approach D to examine the specific binding of human IgG on the sensing film. After Ab_1 was immobilized on activated cGO sheets, mouse IgG-Ab_2FH and bovine IgG-Ab_2FH with the target analytes concentration of 125 ng mL^{-1} were incubated in reactor for 10 min under an external magnetic field. The results show that the resonant wavelengths were almost unchanged after the external magnetic field was switched off and PBS was injected to rinse the sensing film. These experiment results indicate that the fabricated SPR biosensor in this work

has the ability of selective detection of human IgG (Fig. S6). After series of antibody–antigen binding assays were performed, the gold film was regenerated for recycling. We tested the reproducibility of the sensing chip and found that the sensor surface stabilized around 86% initial activities after regeneration for the fifth time (Fig. S7).

3.5 Analysis of real samples

Recovery experiments were performed to examine the feasibility of applying the developed biosensor on real samples. Chicken serums spiked by human IgG with different spiked levels (30, 125 and 500 ng mL^{-1}) were analyzed by approach D. PBS with the same spiked levels of human IgG were also examined as control. The recovery of the present method was defined as the ratio of resonant wavelength shifts caused by injecting chicken serum ($\Delta\lambda_{serum}$) and PBS ($\Delta\lambda_{PBS}$) containing the same spiked level of human IgG. The obtained recoveries ranged from 106% to 117% (Table. S3), which indicates that the non-specific interactions induced by the chicken serum matrix are acceptable, and the developed SPR biosensor based on $FHAb_2$ and cGO had good accuracy and practicability for real samples analysis. It might be the way of injecting separated human IgG from complex serum sample in this design rather than directly injecting complex serum sample to cGO-based sensing chip that leads to

the less matrix interference.

4. Conclusion

In this work, a sensitive SPR sensing strategy was developed for detecting human IgG. Superparamagnetic $FHAb_2$ were used to enrich the target analytes and rapidly deliver the concentrated target analytes from complex samples to the sensing surface under an external magnetic field. Moreover, FH labeling of human IgG could lead to great amplification of SPR signal, owing to the large mass, high refractive index of FH and the strong electromagnetic-field enhancement effect of HGNPs. With the present SPR sensing strategy, the obtained detection limit of human IgG is about 260-fold lower than that obtained by routine sandwich assay. The fabricated SPR biosensor with excellent sensitivity and selectivity shows the potential for detecting various proteins with available corresponding receptors.

.

References

Atar, N., Eren, T., Yola, M.L., 2015. Food Chem. 184, 7–11.

Baghayeri, M., Zare, E.N., Lakouraj, M.M., 2014. Sensor. Actuat. B-Chem. 202, 1200–1208.

Chen, H.X., Hou, Y.F., Ye, Z.H., Wang, H.Y., Koh, K., Shen, Z.M., Shu, Y.Q., 2014. Sensor. Actuat. B-Chem. 201, 433–438.

Eletxigerra, U., Martinez-Perdiguero, J., Barderas, R., Pingarron, J.M., Campuzano, S., Merino, S., 2016. Anal. Chim. Acta 905, 156–162.

Eslamipour, F., Hejazi, P., 2015. J. Mol. Catal. B-Enzym. 119, 1–11.

Garibo, D., Campbell, K., Casanova, A., De la Iglesia P., Fernandez-Tejedor, M., Diogene, J., Elliott, C.T., Campas, M., 2014. Sensor. Actuat. B-Chem. 190, 822–828.

Hedman, J., Klasson M., Nilsson, R., Nordling C., Sorokina, M.F., Kljushnikov, O.I., Nemnonov, S.A., Trapeznikov, V.A., Zyranov, V.G., 1971. Phys. Scripta 4, 195–201.

Hoskins, C., Min, Y., Gueorguieva, M., McDougall, C., Volovick, A., Prentice, P., Wang, Z.G., Melzer, A., Cuschieri A., Wang, L.J., 2012. J. Nanobiotechnology 10, 27.

Kamaruddin, N.H., Bakar, A.A.A., Yaacob, M.H., Mahdi, M.A., Zan, M.S.D., Shaari, S., 2016. Appl. Surf. Sci. 361, 177–184.

Lee, K., Gupta, C.K., Park, S.Y., Kang, I.K., 2016. J. Mater. Chem. B 4, 704–715.

Li, Y., Liu, X., Lin, Z., 2012. Food Chem. 132, 1549–1554.

Liu, S.F., Liu, J., Han, X.P., Cui, Y.N., Wang, W., 2010. Biosens.

Bioelectron. 25, 1640–1645.

Liu, X., Li, L., Liu, Y.Q., Shi, X.B., Li, W.J., Yang, Y., Mao, L.G., 2014. Biosens. Bioelectron. 59, 328–334.

Lopez, A., Lovato, F., Oh, S.H., Lai, Y.H., Filbrun, S., Driskell, E.A., Driskell, J.D., 2016. Talanta 146, 388–393.

Lyon, L.A., Musick, M.D., Natan, M.J., 1998. Anal. Chem. 70, 5177–5183.

Mahmoud, M.A., O'Neil, D., El-Sayed, M.A., 2014. Chem. Mater. 26, 44−58.

Mahmoud, M.E., Ahmed, S.B., Osman, M.M., Abdel-Fattah, T.M., 2015. Fuel 139, 614–621.

Marcus, P., Grimal, J.M., Corros. Sci. 1992. 33, 805–814.

Mariani, S., Scarano, S., Spadavecchia, J., Minunni, M., 2015. Biosens. Bioelectron. 74, 981–988.

Medina-Sanchez, M., Miserere, S., Cadevall, M., Merkoci, A., 2016. Electrophoresis 37, 432–437.

Minamiki, T., Minami, T., Kurita, R., Niwa, O., Wakida, S.I., Fukuda, K., Kumaki, D., Tokito, S., 2014. Materials 7, 6843–6852.

Prabowo, B.A., Su, L.C., Chang, Y.F., Lai, H.C., Chiu, N.F., Liu, K.C., 2016. Sensor. Actuat. B-Chem. 222, 1058–1065.

Schwartzberg, A.M., Olson, T.Y., Talley, C.E., Zhang, J.Z., 2006. J. Phys. Chem. B 110, 19935–19944.

Shi, S., Wang, L.B., Su, R.X., Liu, B.S., Huang, R.L., Qi, W., He, Z.M., 2015. Biosens. Bioelectron. 74, 454–460.

Singh, S., Barick, K.C., Bahadur, D., 2015. Powder Technol. 269, 513–519.

Springer, T., Ermini, M.L., Spackova, B., Jablonku, J., Homola J., 2014. Anal. Chem. 86, 10350−10356.

Sun, Y., Bai, Y.P., Song, D.Q., Li, X.Z., Wang, L.Y., Zhang, H.Q., 2007. Biosens. Bioelectron. 23, 473–478.

Tan, B.J., Klabunde, K.J., Sherwood, P.M.A., 1990. Chem. Mater. 2, 186–191.

Turner, N.H., Single, A.M., 1990. Surf. Interface Anal. 15, 215–222.

Wang, H., Yuan, X.Z., Wu, Y., Chen, X.H., Leng, L.J., Wang, H., Li, H., Zeng, G.M., 2015. Chem. Eng. J. 262, 597–606.

Wang, J.L., Munir, A., Zhu, Z.Z., Zhou, H.S. 2010. Anal. Chem. 82, 6782–6789.

Wang, Q., Liu, R.J., Yang, X.H., Wang, K.M., Zhu, J.Q., He, L.L., Li, Q., 2016. Sensor. Actuat. B-Chem. 223, 613–620.

Wang, Y., Dostalek, J., Knoll, W., 2011. Anal. Chem. 83, 6202–6207.

Wu, Q., Sun, Y., Ma, P.Y., Zhang, D., Li, S., Wang, X.H., Song, D.Q., 2016. Anal. Chim. Acta 913, 137–144.

Wu, X.L., Li, Y., Liu, B., Feng, Y., He, W.Y., Liu, Z.G., Liu, L.Z., Wang, Z.M., Huang, H.Z., 2016. Food Anal. Method. 9, 582–588.

Yao, G.H., Liang, R.P., Huang, C.F., Wang, Y., Qiu, J.D., 2013. Anal. Chem. 85, 11944−11951.

Yuk, J.S., Guignon, E.F., Lynes, M.A., 2013. Analyst 138, 2576–2582.

Zhang, D., Sun, Y., Wu, Q., Ma, P.Y., Zhang, H., Wang, Y.P., Song, D.Q., 2016. Talanta 146, 364–368.

Zhang, H., Sun, Y., Gao, S., Zhang, H.Q., Zhang, J., Bai, Y., Song, D.Q., 2014. Talanta 125, 29–35.

Zhang, J., Sun, Y., Wu, Q., Gao, Y., Zhang, H., Bai, Y., Song, D.Q., 2014. Colloid. Surface. B. 116, 211–218.

Zhong, X., Chai, Y.Q., Yuan, R., 2014. Talanta 128, 9–14.

Zhang, X.N., Zhang, F., Zhang, H.Y., Shen, J.Z., Han, E., Dong, X.Y., 2015. Talanta 132, 600–605.

Figure captions

Fig. 1. Schematic diagram of experimental procedure.

Fig. 2. TEM images of Fe_3O_4 NPs (a), HGNPs (b), Fe_3O_4-HGNPs nanohybrids (c) and photographic images of Fe_3O_4-HGNPs nanohybrids in the absence and presence of an external magnetic field (d).

Fig. 3. Magnetization curves of Fe_3O_4 NPs and Fe_3O_4-HGNPs nanohybrids.

Fig. 4. UV-Vis absorption spectra of Fe_3O_4 NPs (a), HGNPs (b), Fe_3O_4-HGNPs nanohybrids (c) and Fe_3O_4-HGNPs-Ab_2 (d).

Fig. 5. Kinetic adsorption curves of rabbit anti-human IgG at different concentrations on cGO-modified gold film (a) and relationships between concentrations of human IgG and shifts of resonant wavelengths obtained by routine sandwich assay approach (A), Fe_3O_4 NPs-Ab_2-enhanced sandwich assay approach (B), Fe_3O_4-HGNPs-Ab_2-enhanced sandwich assay approach (C) and Fe_3O_4-HGNPs-Ab_2-enhanced sandwich assay approach with an external magnetic field approach (D). Error bar =±S.D. and n = 3.

Table captions

Table 1. Comparison with reported immunoassay methods.

Method	Analytes	Detection limit	References
Wavelength modulation SPR biosensor	Human IgG	1.88 ng mL^{-1}	Present work
Optical fiber SPR biosensor	Human IgG	2 μg mL^{-1}	Shi et al., 2015
Field effect transistor-based biosensor	Bovine IgG	0.62 μg mL^{-1}	Minamiki et al., 2014
Wavelength modulation SPR biosensor	Mouse IgG	0.6 μg mL^{-1}	Zhang et al., 2016
LC microdroplet-based biosensor	Rabbit IgG	16 ng mL^{-1}	Lee et al., 2016
Disposable Microfluidic platform	Human IgG	3.5 ng mL^{-1}	Medina-Sanchez et al., 2016
	Mouse IgG		Lopez et al., 2016
SERS immunoassay	Mouse IgG	1.9 ng mL^{-1}	Liu et al., 2016
Portable SPR optical	Human	40.3 pg	Lynes et al.,

biosensor	IgG	mL^{-1}	2013
Grating coupler-based SPCE biosensor		1 pg mL^{-1}	

Table. 1

Highlights

- SPR spectroscopy is coupled with magnetic bioseparation technique for immunoassay.
- Magnetic nanohybrids are served as "vehicles" for rapid target analyte delivery from a sample solution to the sensor surface via magnetic driven mass transfer.
- Fe_3O_4-hollow gold nanohybrids as labels significantly amplify the SPR response.
- The detection limit achieved by the present method for detecting human IgG is about 260 times lower than that obtained by routine sandwich assay.